EASR

Engineering and Applied Science Research

https://www.tci-thaijo.org/index.php/easr/index

Published by the Faculty of Engineering, Khon Kaen University, Thailand

Microstructural and mechanical behavior of friction stir welded AZ31-AZ61 magnesium alloys dissimilar joint

Ahmed Kellai*[1)], Liamine Kaba[1)], Seddik Ouallam[1)], Said Dehimi[1)], Sami Kahla[1)], Mohammed Elamine Djeghlal[2)] and Tarek Bendris[1)]

[1)]Research Center in Industrial Technologies, Chéraga 16014, Algiers, Algeria
[2)]Departments of Metallurgy, Polytechnic National School (ENP), El Harrach 16200, Algiers, Algeria

Received 10 January 2024
Revised 11 June 2024
Accepted 14 June 2024

Abstract

In this work, the effect of high tool rotation speed (ω) and forward velocity (V) in dissimilar friction stir welding (FSW) of AZ31-AZ61 magnesium alloys thin plates on microstructural and mechanical properties was studied. The results reveal a continuous dynamic recrystallization and grain refinement in the stir zone (SZ) with formation of precipitates particles Al_8Mn_5 and some undissolved intergranular compounds β-$Al_{12}Mg_{17}$. Also, the microstructures of both thermo-mechanically affected zones $TMAZ_{AZ31}$ and $TMAZ_{AZ61}$ consist of elongated restored grains generally coarser than those found in SZ. The heat affected zone (HAZ) exhibits the same grains appearance as those of base metals (BMs). The stir zone displays the highest microhardness with 60 HV and 68 HV for both sides of the weld joint AZ31 and AZ61, respectively. The ultimate tensile strength (UTS) of the welded joint improves, reaching values of 75.77% for AZ31 base materials and 63.55% for AZ61 base materials.

Keywords: Friction stir welding, Magnesium alloy, Intermetallic compounds, Microstructure, Mechanical property

1. Introduction

The pursuit of weight reduction, aimed at saving energy and mitigating environmental impact by curbing fuel emissions, is a major research focus in many industries. Lightweight structural materials have great potential for weight saving applications and make them highly sought-after raw material for numerous applications including aerospace, aeronautics, automotive, electronics and various other industries. Magnesium and its alloys are considered among the most important light metals due to their numerous distinctive advantages. These include having two-thirds (2/3) the density of aluminum, ease of recyclability, and high mechanical properties. However, its crystalline structure compromises its ductility, formability, and ability to withstand room temperature [1-3]. In most cases, magnesium alloys exhibit ternary behavior, with major alloying elements including aluminum, zinc, thorium and rare earths. Aluminum plays a primary role in the ternary Mg–Al series, which includes AZ (Mg–Al–Zn), AM (Mg–Al–Mn) and AS (Mg–Al–Si) alloys [4, 5]. The addition of zinc improves castability and slightly enhances corrosion resistance, but also leads to increased microporosity and hot cracking, limiting thereby its content to a maximum of 3 % [6]. Hence, cutting and joining are an imperative technical requirement to prevent deformation of these alloys, which results in a reduction in formability when producing mechanical designs. For this reason, welding is considered the best solution.

A variety of welding methods have been employed to join magnesium alloy components, including tungsten inert gas (TIG), metal inert gas (MIG) and plasma arc processes, laser [7], electron, friction [8], explosion, adhesive [9], stud, ultrasonic [10], and spot welding [11]. Currently, TIG and MIG processes are the main techniques for magnesium alloys, particularly for the removal and repair of casting defects [12]. However, these techniques pose several challenges, including cracks, porosity, high oxidation rates, low welding speeds, large heat affected zone (HAZ) and weld zone (WZ), poor microstructural and mechanical properties, evaporative loss of alloying elements, as well as high residual stress and deformation of welded joints [13-15]. Moreover, the welding defects caused by conventional welding greatly reduce the performance especially for dissimilar welding of magnesium alloys [16]. This is why numerous studies have shown that the FSW process is the most recommended for this type of welding due to its numerous advantages.

Friction stir welding (FSW) is a relatively new solid-state joining process invented and patented in 1991 by Wayne Thomas, at The Welding Institute (TWI). Its primary objective was to eliminate the defects inherent in fusion welding processes, particularly in aluminum and magnesium alloy assemblies [17]. Currently, a number of research projects have been carried out using this technique (FSW) to investigate the welding of magnesium alloys. For instance, Patel et al. [18] and Kumar and Vanitha [19] reported that FSW modifies the microstructure of the base material and leads to the formation of weld nugget/stir zone (SZ), thermo-mechanically affected zone (TMAZ) and heat affected zone (HAZ). Singh et al. [5] and Çam [20] reported that each zone of the FSW joint has distinct microstructural characteristics, such as grain shape, grain size, dislocation density, precipitate shape and residual stress distribution. Ahmed et al. [21] and Mironov et al. [22] clarified that the SZ area undergoes a thermomechanical cycle that allows the dynamic recrystallization process to occur, resulting in the formation of a new equiaxed fine-grained structure. TMAZ also undergoes a

*Corresponding author.
Email address: kellai.a.a@gmail.com
doi: 10.14456/easr.2024.47

thermomechanical cycle, but this does not allow recrystallization and produces only geometrically deformed grains, mainly due to the passage of the tool with a high density of substructures. Singh et al. [5] and Esparza et al. [23] demonstrated that HAZ does not undergo recrystallization; instead, it experiences thermal cycling, affecting existing precipitates and exhibiting an elongated shape depending on the initial tempered state of the base metal. This region remains unaffected by the rubbing of the shoulder or the stirring of the pin during the welding process. Lee et al. [24] reported that the ultimate tensile strength of the AZ31B -H24 alloy joint increased with increasing tool rotation speed and with decreasing welding speed. However, the maximum joint strength reached 85 % of that of the base metal. Singh et al. [25] found that the grains of the AZ61 base metal were recrystallized in the mixing zone and in the transition zone during welding. Thimmaiah et al. [26] found that the ZK60 alloy joint exhibited excellent tensile properties after compression perpendicular to the welding direction and ageing treatment. Zhang et al. [27] reported that in dissimilar welding of AZ31-AM60 magnesium alloys, the grains size of AZ31 was smaller than that of AM60 in the SZ with a high localized texture. In their study, Zhou et al. [28] used the FSW process to weld two magnesium alloys AZ40M and AZ61A and found that the SZ had an equiaxed fine-grained microstructure with formation of Al_8Mn_5 and $Mg_{17}Al_{12}$ type precipitate. This region displayed improved corrosion resistance compared to the base metal (BM). Conversely, Singh and Dubey [29] demonstrated, under well-defined FSW dissimilar welding conditions of AZ31-AZ91 alloys, that SZ exhibited a granular microstructure. The latter was coarser on the AZ91 side compared to AZ31 side. Additionally, Yu et al. [30] noted that grains formed through dynamic recrystallization in this region. Second-phase particles observed in this region were small. The ultimate tensile strength of the AZ31/AZ61 weld seam reached 96.1% of that of the AZ31 base metal BM. Finally, Singh et al. [31] assessed the effects of post-weld heat treatment PWHT on AZ61 alloy FSW joints. After post-weld heat-treatment (PWHT), they observed a slight improvement in tensile strength, accompanied by an approximately 18.5 % increase in weld joint elongation.

AZ31 and AZ61 magnesium alloys find extensive use in various fields due to their low density, high strength, and good corrosion resistance. Unfortunately, they pose significant challenges when used in fusion welding processes. Therefore, it is imperative to investigate the FSW characteristics of these alloys particularly given the limited research on this subject. In this paper, we are interested in studying the effect of high tool rotation speed (ω) and forward velocity (V) in FSW dissimilar welding of AZ31-AZ61 magnesium alloys on the microstructural and mechanical behavior.

2. Materials and methods

The base materials used are AZ31 and AZ61 type magnesium alloy sheets with dimensions of 150 x 150 x 2 mm. These alloys possess good rolling properties. They are typically hot-rolled in several passes, then adjusted and annealed at 300 °C (AZ31) and 250 °C (AZ61). Chemical analyses of the materials used were carried out by spark erosion spectrometer brand: OXFORD model: FOUNDRY MASTER PRO, and summarizes in Table 1. The sheets to be welded were cleaned with a stainless-steel wire brush to remove the oxide layer (MgO) and stripped with acetone to eliminate any grease. As shown in Figure 1, welding was carried out along the rolling direction of the BMs. FSW equipment (EADS-IWF MTS Istir PDS) was used for the welding joint. The FSW tool consisted of a shoulder with a diameter of 10 mm and a cylindrical stirring pin with a diameter and length of 4 and 1.8 mm, respectively. The shoulder plunge depth was 0.2 mm. The parts were butt-jointed using a clamping system and assembled using the welding parameters shown in Table 2.

Table 1 Chemical composition of base materials

	Chemical Composition (Wt %)							
Material	***Al***	***Zn***	***Mn***	***Si***	***Cu***	***Ni***	***Fe***	***Mg***
AZ31	3.46	0.43	0.17	0.022	0.012	0.005	0.045	Bal.
AZ61	5.95	0.43	0.32	0.006	<0.002	0.002	0.002	Bal.

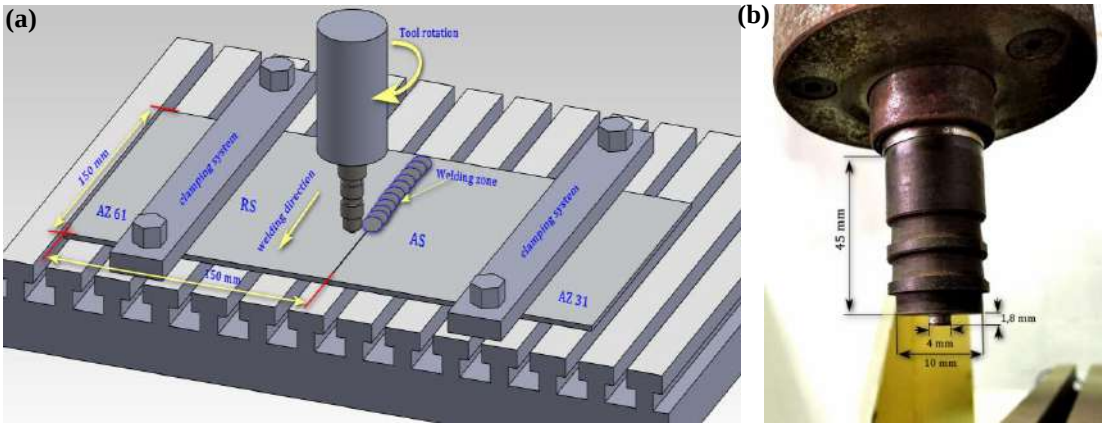

Figure 1 (a) FSW process graphical representation, (b) Physical photos of pin

Table 2 Welding parameters

Pin diameter (mm)	Shoulder diameter (mm)	Rotation speed ω (rpm)	Forward velocity V (mm/min)
4	10	1600	600

Samples for metallographic observations were cut on the cross-section perpendicular to the welding direction. They were then embedding with cold acrylic resin (VersoCit-2 Powder mixed with VersoCit-2 Liquid) and polished using a series of abrasive papers ranging from 220 to 4000, and finally finished with felt paper and a diamond suspension of 3 and 1 µm. To reveal the microstructures of the different zones within the weld joint, we utilized a reagent consisting of an acetic glycol solution with the following composition: 19 (ml) water, 60 (ml) ethylene glycol, 20 (ml) acetic acid and 1 (ml) HNO_3. Microstructural observations were performed using Nikon-type optical microscopy and a scanning electron microscope SEM (ZEISS.EVO-MA 25) equipped with a microanalysis system (EDS). The grains size was measured using image J software and Line intercept method in accordance with ASTM E112–10. The X-ray diffraction (XRD) technique was employed to evaluate the phases present in the BM. The diffractometer used was a BRUKER D2 PHASER 2G mark equipped with a copper (Cu) anticathode delivering an X-ray wavelength of 1.5406 nm, an acquisition step of 0.02 °, a voltage V = 30kV and an intensity I = 10mA. Mechanical behavior was primarily assessed through tensile and micro-hardness tests. The tensile test was performed at room temperature using an MTS Criterion Model 45 hydraulic test machine with a tensile speed of 0.05 mm/s. Tensile test specimens machined in accordance with ASTM E8-04 standard. The micro-hardness test was conducted using an automatic BUEHLER WILSON VH3300 machine with a 300 g loading force and a 300 µm pitch.

3. Results and discussion

3.1 Macro examination

Figure 2 shows the visual appearance of the weldment of AZ31-AZ61 magnesium alloys produced by FSW process, with distinct high and down sides: AZ31 on the advancing side (AS), and AZ61 on the retreating side (RS). It can be noted that the weld joint exhibits a satisfactory appearance, characterized by good superposition of the shoulder streaks and uniform width along the joint.

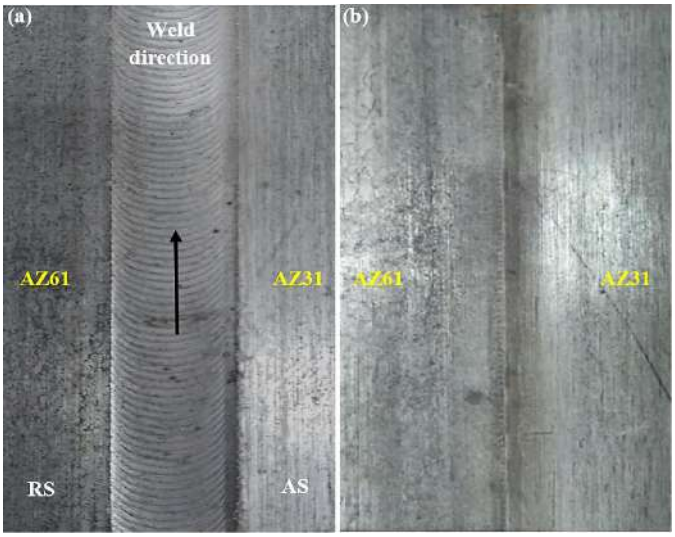

Figure 2 Visual appearance of the AZ31-AZ61 FSW weld joint: (a) top side, (b) bottom side

Figure 3 illustrates a macroscopic cross-section of the weld seam. It can be seen that the joint has a highly heterogeneous microstructure, with four distinct main zones: the stir zone (SZ), the thermos-mechanically affected zone (TMAZ), the heat affected zone (HAZ), and finally the unaffected base metal (BM). The SZ is composed of two distinct sub-regions from AS to RS, namely SZ_{AZ31} and SZ_{AZ61}. This microstructural modification is generally associated with the temperature gradients and mechanical effect of the tool mixing characteristic of the FSW process. SZ undergoes a reduction in grain size due to a very high rate of plastic deformation with a temperature rise of up to 500 °C. The microstructures of TMAZ undergo significant plastic deformation at temperatures of around 400-450 °C. The HAZ experiences a thermal cycle without mechanical deformation with temperatures ranging from 20 to 400 °C [16, 18].

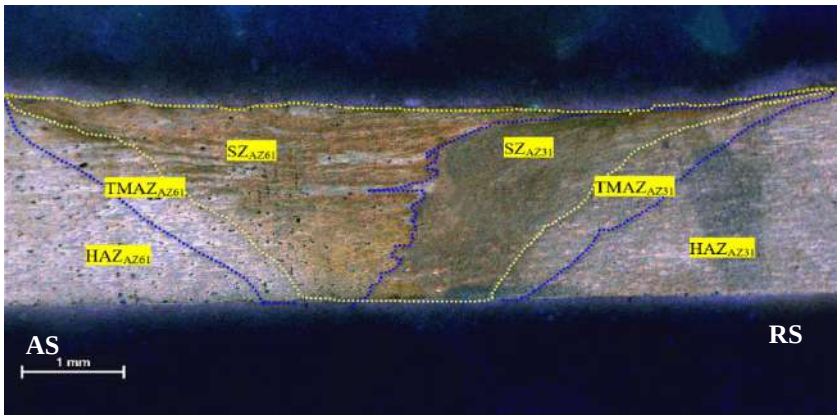

Figure 3 Optical macrograph of the weld joint

3.2 Microstructure examination

The microstructures of AZ31 and AZ61 base metals are depicted in the optical micrographs of Figure 4. These microstructures consist primarily of an α-Mg phase matrix with fine polyhydric structure, and two types of intermetallic compound particles (Al_8Mn_5, and β-$Al_{12}Mg_{17}$) which are clearly visible either at the grain boundaries or within the grains, and are less than 1μm. The Al_8Mn_5 intermetallic phases are generally formed in most commercial Mg-Al alloys [32-34], as revealed by the XRD analysis (Figure 5) and EDS analysis (Figure 6). It can also be seen that the microstructure of AZ31 base metal has a larger average grain size (17.791 μm) than that of the AZ61 base metal (16.424 μm), as calculated from the diagrams in Figure 7. This difference in grain size can be attributed to the heat treatment they have undergone and their respective chemical compositions. The varying values of grain size for different regions of the weldment are summarized in Table 3.

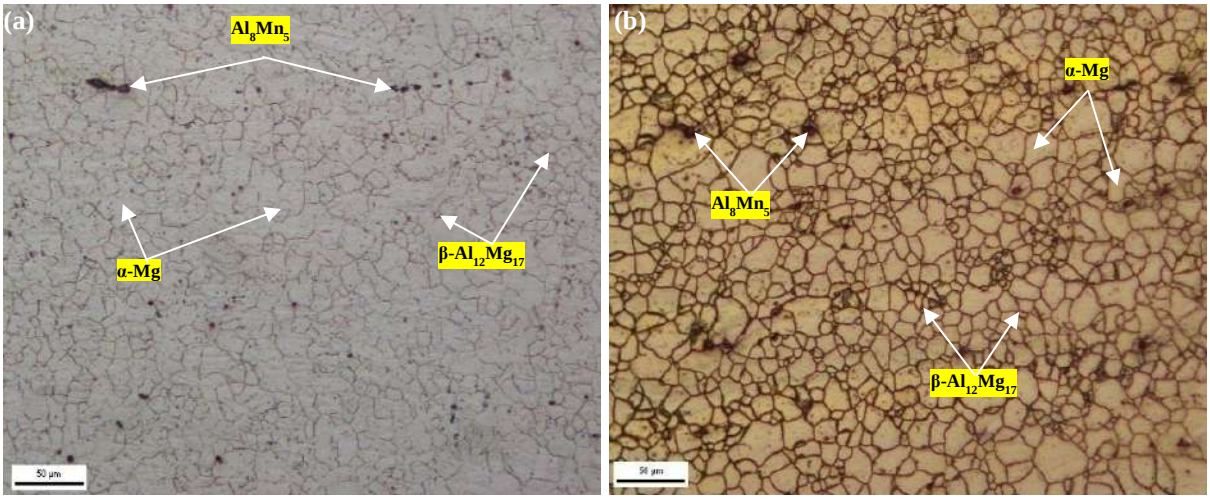

Figure 4 Optical micrographs of base metal: (a) AZ31, (b) AZ61

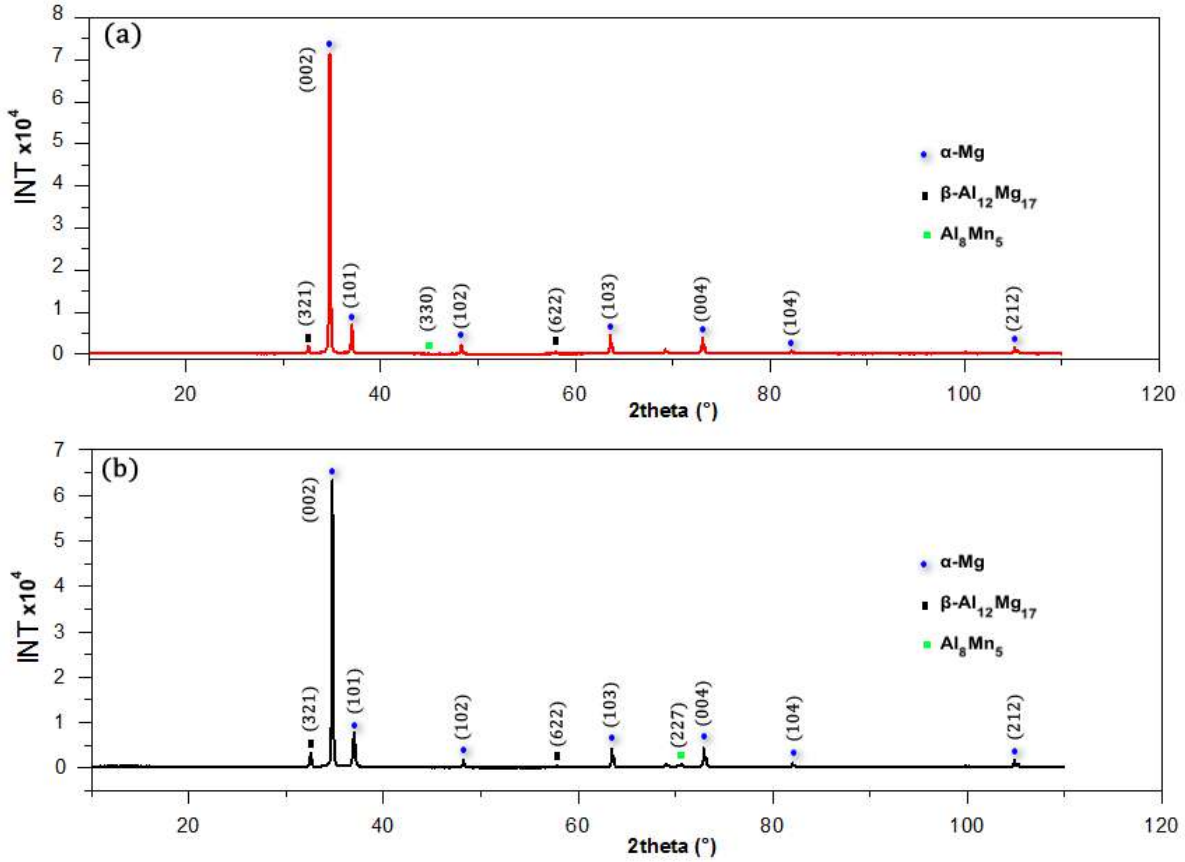

Figure 5 X-ray diffraction (XRD) spectra of base metals: (a) AZ31, (b) AZ61

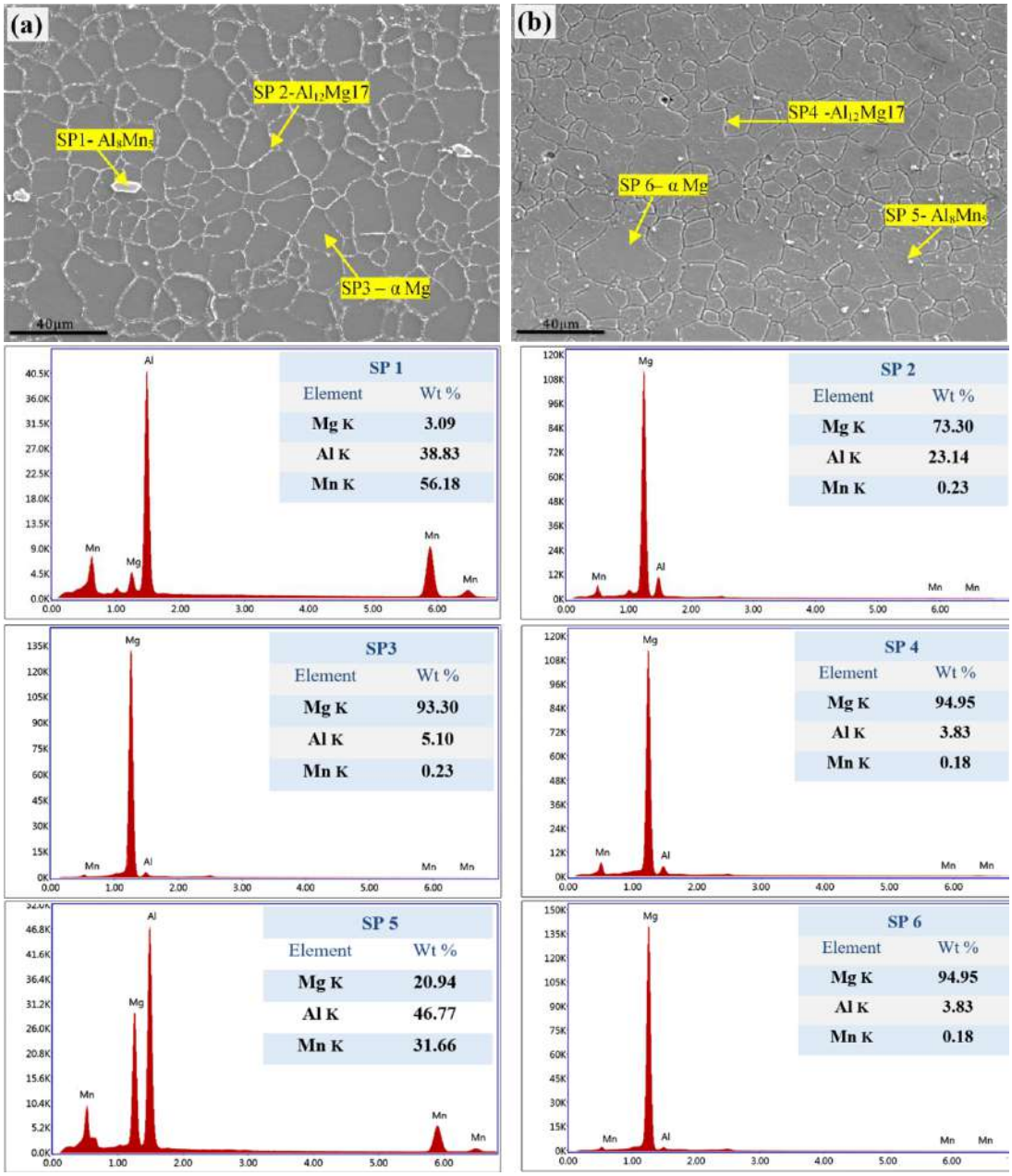

Figure 6 SEM/EDS images shows BM of both Mg alloys: (a) AZ31, (b) AZ61

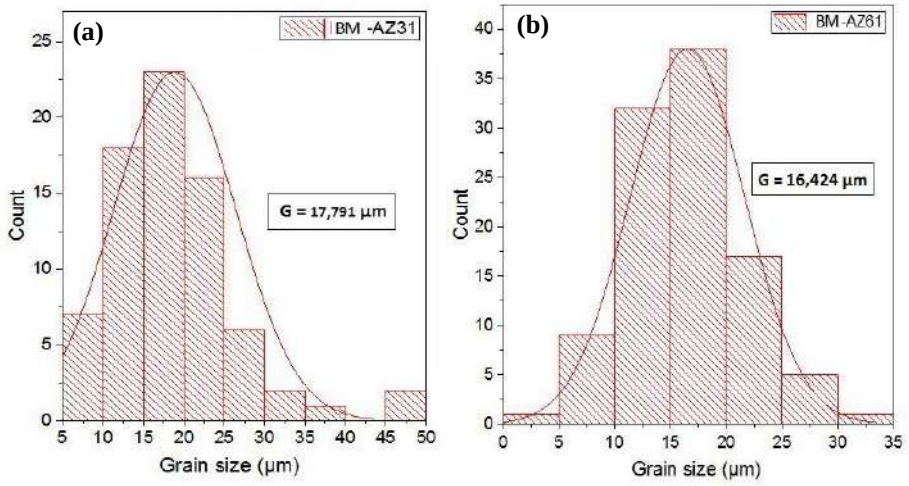

Figure 7 Typical estimate of the grain size for various regions of the joint: (a) AZ31, (b) AZ61

Table 3 Average grain size in various regions of the welded joint

	AZ31				AZ61			
	BM	***HAZ***	***TMAZ***	***SZ***	***BM***	***HAZ***	***TMAZ***	***SZ***
Grain size (µm)	17.791	17.905	16.194	3.070	16.424	16.904	17.529	3.002

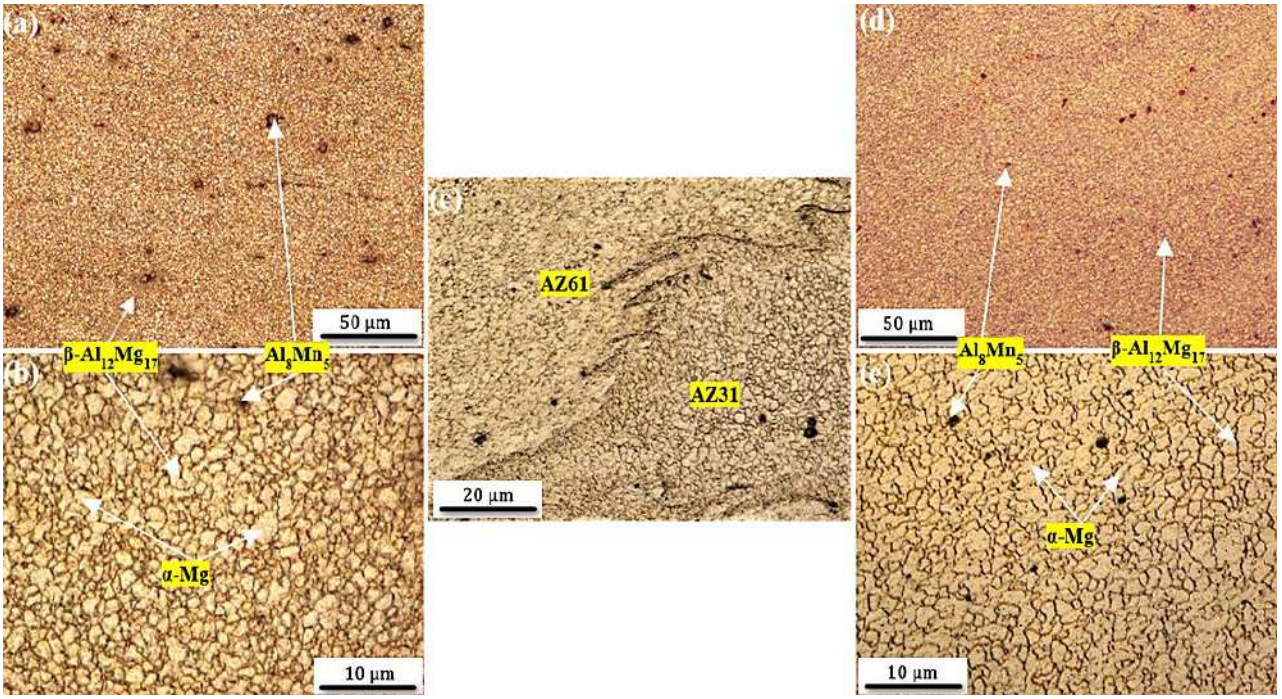

Figure 8 Optical micrographs of stir zones SZ_{AZ61}-SZ_{AZ31}

The microstructures of the stir zones SZ_{AZ61}-SZ_{AZ31} at different scales are shown in Figure 8(a-e). It can be clearly seen that the stir zone of both alloys AZ61 (Figure 8(a, b)), and AZ31 (Figure 8(d, e)) are characterized by a uniform and very fine equiaxed grains morphology with an average size of 3 µm. Notably, this grain size is significantly smaller than that of base metals. This reduction is attributable to the a very high rate of plastic deformation with a temperature rise of up to 500 °C [35]. Furthermore, the combined effects of temperature and plastic deformation in FSW produce recrystallization, precipitation and texture evolution. Small, weakly disoriented sub-grains are formed by a rearrangement of dislocations with an increase in temperature. The continuous introduction of dislocations into these sub-grains leads to dynamic recrystallization, resulting in grain refinement. Grain refinement associated with recrystallization depends on several parameters, including tool rotation speed (ω) and forward velocity (V). These parameters influence temperature, strain rate and then the size of recrystallized grains, particularly in the SZ zone where the maximum temperature was recorded. Decreasing the tool rotation speed at a constant forward velocity or decreasing ω/V resulted in a reduction in SZ grain size [36-38]. Figure 8c shows the interface between SZ_{AZ31} and SZ_{AZ61}, demonstrating that the grain size on the AZ31 side is greater than that on the AZ61 side due to the higher temperature of the AS than the RS [30, 39]. It is also noted that formation of precipitates particles Al_8Mn_5 and intergranular compounds β-$Al_{12}Mg_{17}$ with a high rate on the AZ61 side as shown in EDS analysis (Figure 9).

Figure 10 illustrates the microstructures of thermo-mechanically affected zones TMAZ for both parts of the weld joint, where these regions undergo insufficient plastic deformation at temperatures in the range 400-450 °C. The microstructures of both $TMAZ_{AZ31}$ (Figure 10a) and $TMAZ_{AZ61}$ (Figure 10b) undergo a restoration process with low-angle disorientation joints and high density of dislocations. This is due to the partial recrystallization occurring in the bonded regions directly from the stir zone, where thermal exposure and plastic deformation are insufficient [36, 40]. Its grains shape is elongated due to plastic deformation generated by the material flow created by the tool, which can go up to 90° next to the core [36]. The grain size in the TMAZ is coarser than that in SZ area [5]. It can be observed that the grains size in TMAZ range from 2 to 20 µm for both sides. However, it is noteworthy that the grain size of $TMAZ_{AZ61}$ is coarser than that of $TMAZ_{AZ31}$. This variation is due to the grain restoration and tool rotation direction during welding operation [41].

The heat affected zones HAZ_s are shown in Figure 11. These zones experience a thermal cycle without mechanical deformation with temperatures ranging from 20 to 400 °C. In contrast, the matrix only undergoes over-tempering characterized by a continuous change in the precipitation state from one end of the HAZ to the other [42, 43]. It can be seen that the grains retain the same appearance as those of the base metals. This can be explained by the history of these alloys, as they have previously undergone a 300 °C heat treatment.

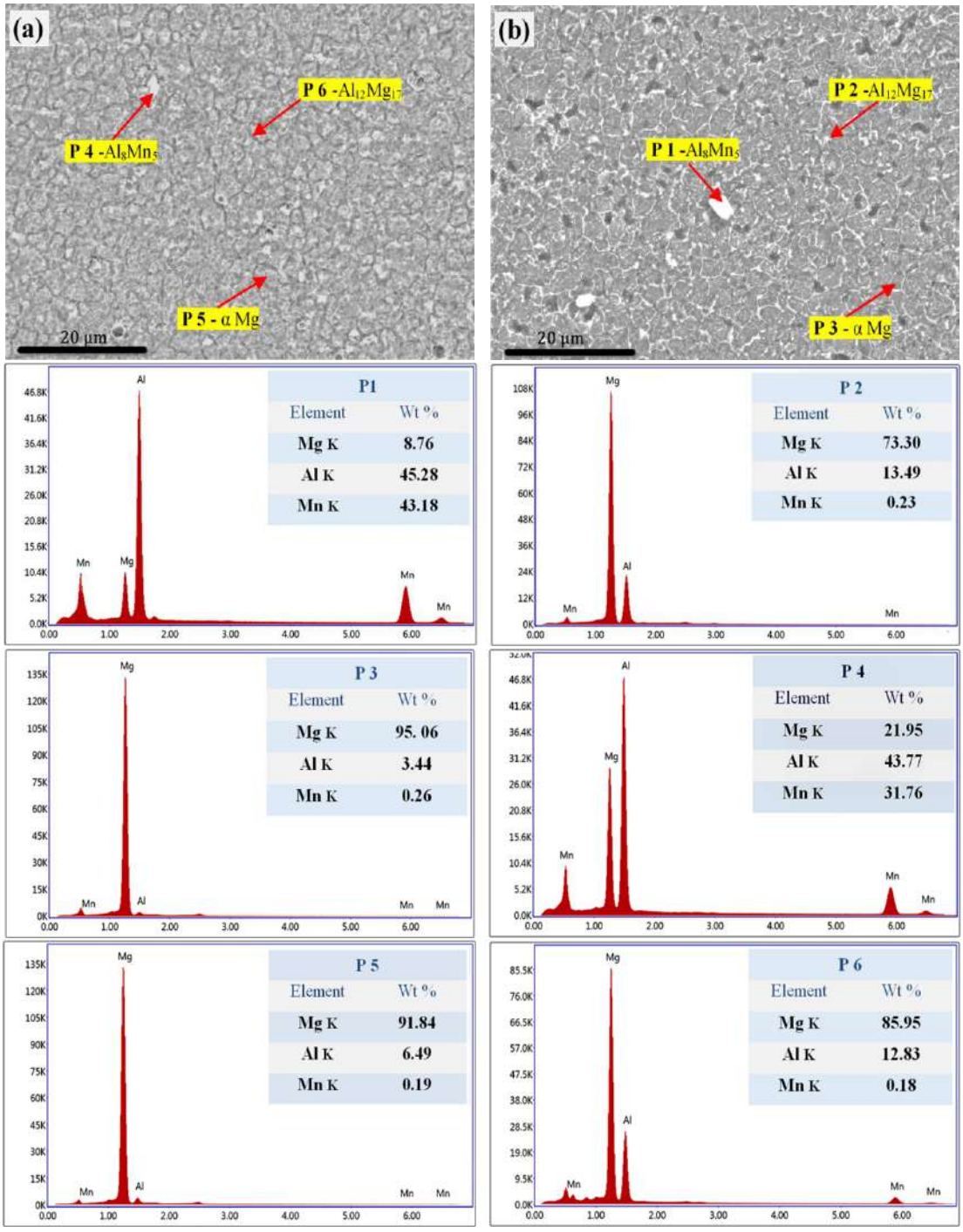

Figure 9 SEM/EDS images shows SZ of both Mg alloys: (a) AZ61, (b) AZ31

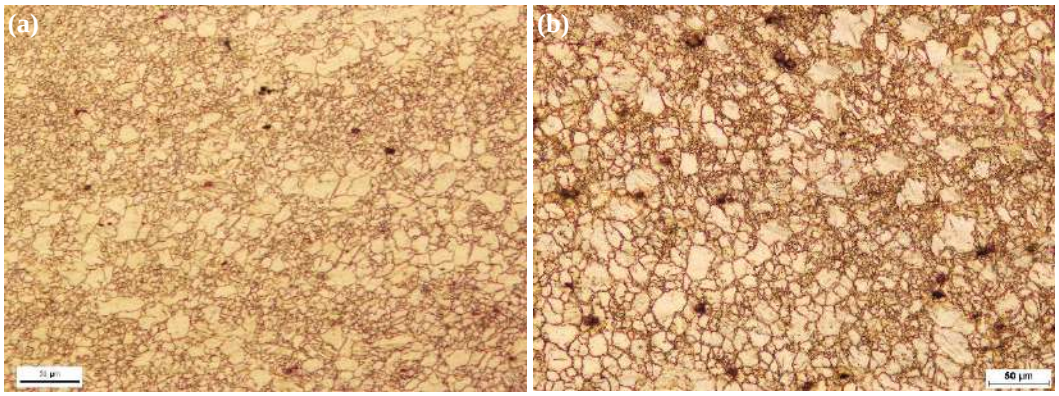

Figure 10 Optical micrograph of thermos-mechanically affected zones: (a) $TMAZ_{AZ31}$, (b) $TMAZ_{AZ61}$

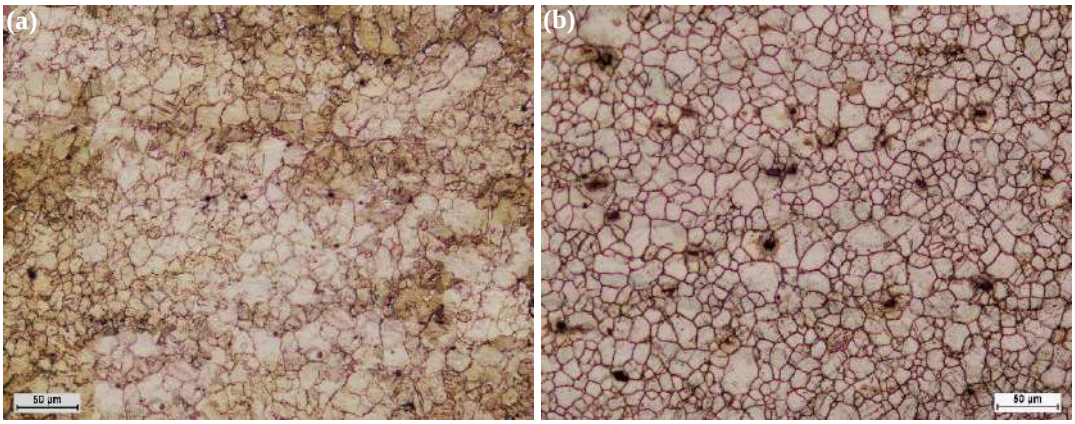

Figure 11 Optical micrograph of heat-affected zones: (a) HAZ_{AZ31}, (b) HAZ_{AZ61}

3.3 Mechanical properties

3.3.1 Micro-hardness testing

The micro-hardness profiles of the AZ31-AZ61 FSW weld joint is illustrated in Figure 12. High values are recorded in the stir zone (SZ) of about 70 HV relative of the base metal and other zones. This is attributable to the fine grain structure which can result in the presence of a large number of grain boundaries, high dislocation density and the presence of hard $Mg_{17}Al_{12}$ phase [5, 35, 44]. Also, there is a clear difference between the SZ near the AZ31 and the SZ near the AZ61 due to the influence of grains size, dislocation density, residual stress variations and presence of the crystallographic texture [5, 30]. It has been reported that the micro-hardness in the thermos-mechanically affected zones TMAZs and in the HAZs of the joint decreased gradually, in the $TMAZ_{AZ61} \approx 64$ and in the $TMAZ_{AZ31} \approx 56$ HV. The decrease in the hardness was due to the larger grain size [5, 16, 30]. The micro-hardness in the HAZ, near to the TMAZ for AZ61 side is the same as the base metal and sometimes slightly higher, which is due to the presence of precipitates.

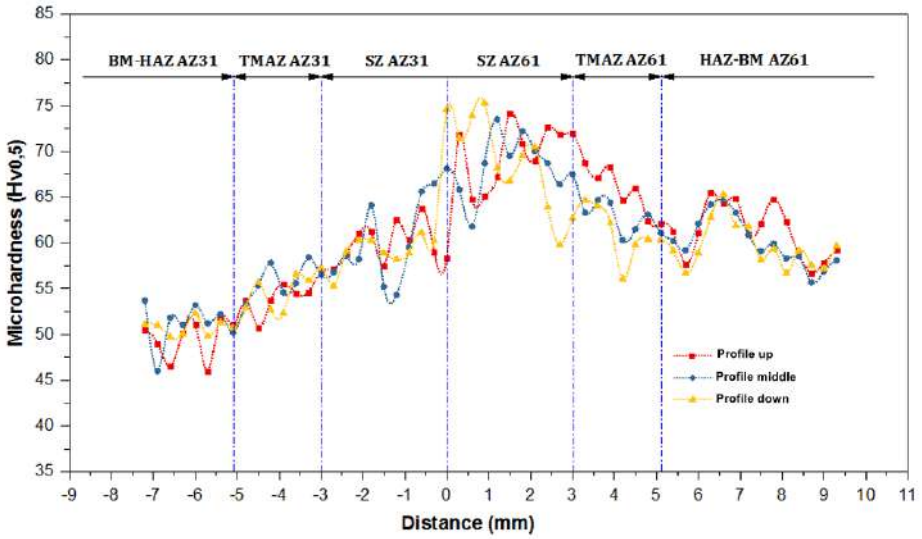

Figure 12 Micro-hardness profile in different zones of the weld joint

3.3.2 Tensile testing

The tensile behavior of magnesium alloys AZ31 and AZ61, as well as the dissimilar FSW joint between them, is illustrated in Figure 13. The detailed characteristics of ultimate tensile strength (UTS), yield strength (YS) and elongation are provided in Table 4. The results show that both the AZ31 and AZ61 alloys exhibit good elongation and almost identical, high tensile strength (310 MPa). These results indicate that both types of alloys exhibit virtually the same plastic deformability, as evidenced by their shear fractures at 45° [45-47]. The dissimilar joint obtained by FSW has poor overall tensile properties, due to the grain structure and brittleness of the intermetallics compounds (IMCs) [16, 48, 49]. Tensile tests show 36 % and 24 % reduction in the strength of the welded joint compared to the AZ61 and AZ31 base metals, respectively. Figure 14 presents the tensile specimen both before and after the test. It can be clearly seen that the tensile fracture occurred on the AZ31-SZ side, which is logical considering the higher UTS of AZ61 compared to AZ31. Clear dimples were detected in Figures 15a and b, indicating that both the weld and the AZ31 tensile samples exhibited ductile fractures. The dimples observed on the AZ31 tensile sample were of greater size compared to those found on the AZ31-AZ61 welded sample. The reason for this phenomena is the significantly greater grain size of the AZ31 BM in comparison to that of the SZ [30, 48, 50].

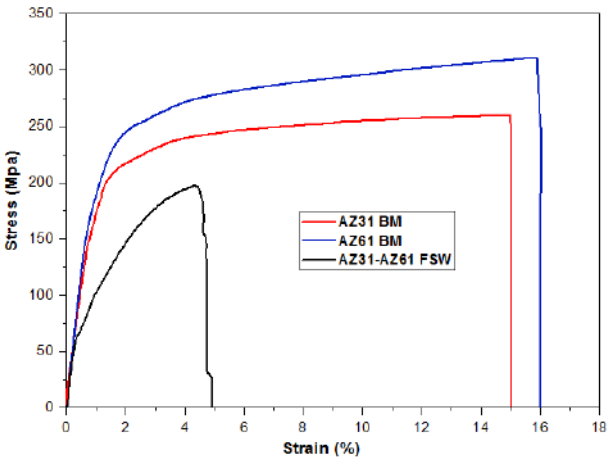

Figure 13 Stress–strain curves of Mg samples at room temperature

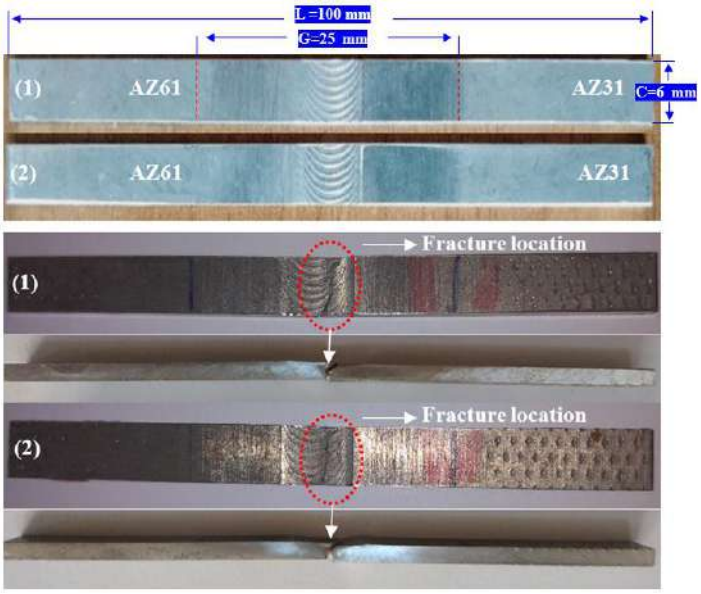

Figure 14 Tensile tested samples

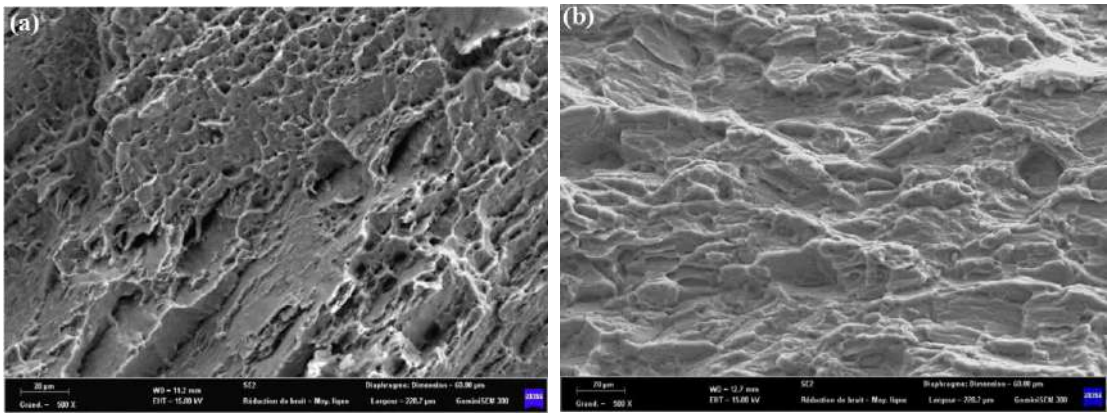

Figure 15 SEM images showing fracture surfaces of the tensile samples: (a) AZ31-AZ61 welded joint, (b) AZ31BM.

Table 4 Mechanical properties of tensile tests

Specimen	Ultimate tensile strength (MPa)	Yield strength 0.2% (MPa)	Elongation (%)
AZ31	260	200	15
AZ61	310	230	16
AZ31-AZ61	197	92	4.93

4. Conclusion

The main following conclusions of this work can be made:

1. In FSW dissimilar welding of AZ31-AZ61 magnesium alloy thin plates, high tool rotation speed and forward velocity play an essential role in fabricating good welds without defects.
2. The tool pin diameter and geometry, and shoulder diameter significantly affected the joint properties. The friction induced among the work piece & tool shoulder is the prime factor responsible for heat produced in FSW.
3. During FSW process, base metal microstructure is modified and lead to the formation of SZ, TMAZ and HAZ. Every zone contains different microstructure, grain size, and precipitate shape and rate. SZ has a uniform and very fine equiaxed grains morphology (~3µm) with a redistributed intergranular precipitation formed β-$Al_{12}Mg_{17}$ after its broken operation throughout the matrix due to the tool rotation. The microstructure of TMAZ consist of elongated restored grains generally coarser than those found in SZ. The HAZ exhibits the same grains appearance as those of BM.
4. The micro-hardness of the joint fluctuated between 50 and 75 HV. The higher hardness in the stir zone is due to the fine grain structure which can result in the presence of a large number of grain boundaries, high dislocation density and the presence of hard $Mg_{17}Al_{12}$ phase.
5. The UTS of the weld joint reached 75.77 % of the AZ31, and 63.55 % of the AZ61 base materials. The tensile joints fractured on the AZ31-SZ side due to the higher UTS of the AZ61 compared with the AZ31.

5. Acknowledgements

The authors wish to express their sincere appreciations to the Research Center in Industrial Technologies (CRTI).

6. References

[1] Xu T, Yang Y, Peng X, Song J, Pan F. Overview of advancement and development trend on magnesium alloy. J Magnes Alloy. 2019;7(3):536-44.
[2] Rios JM, Restrepo AH, Zuleta AA, Javier Bolívar F, Castaño JG, Correa E, et al. Effects of two-step high-energy ball milling process and hot isostatic pressing on the mechanical properties of PM magnesium. Int J Adv Manuf Technol. 2022;121(1-2):187-96.
[3] Lapointe D. Conception d'un dossier de siège d'autobus en aluminium hydroformé [dissertation]. Québec, Canada: Laval University; 2010. (In French)
[4] Dargusch MS, Dunlop GL, Bowles AL, Pettersen K, Bakke P. The effect of silicon content on the microstructure and creep behavior in die-cast magnesium AS alloys. Metall Mater Trans A. 2004;35:1905-9.
[5] Singh K, Singh G, Singh H. Review on friction stir welding of magnesium alloys. J Magnes Alloy. 2018;6(4):399-416.
[6] Pommiers S, Frayret J, Castetbon A, Potin-Gautier M. Alternative conversion coatings to chromate for the protection of magnesium alloys. Corros Sci. 2014;84:135-46.
[7] Cao XJ, Jahazi M, Immarigeon JP, Wallace W. A review of laser welding techniques for magnesium alloys. J Mater Process Technol. 2006;171(2):188-204.
[8] Haferkamp H, Burmester I, Niemeyer M, Doege E, Droder K. Innovative production technologies for magnesium light-weight constructions-Laser beam welding and sheet metal forming. Proceedings of the 30th international symposium on automotive technology and automation; 1997 Jun 16-19; Florence, Italy. p. 247-58.
[9] Westengen H. Magnesium die casting: from ingots to automotive parts. Light Metal Age. 2000;58:44-53.
[10] Busk RS. Magnesium Products Design. New York: Marcel Dekker Inc; 1987.
[11] Manladan SM, Yusof F, Ramesh S, Fadzil M. A review on resistance spot welding of magnesium alloys. Int J Adv Manuf Technol. 2016;86:1805-25.
[12] Marya M, Edwards G, Marya S, Olson DL. Fundamentals in the fusion welding of magnesium and its alloys. Proceedings of the seventh JWS international symposium; 2001 Nov 20-22; Kobe, Japan. p. 597-602.
[13] Salamati M, Soltanpour M, Fazli A. Processing and tooling considerations in joining by forming technologies; part B—friction-based welding. Int J Adv Manuf Technol. 2020;106:4023-81.
[14] Kaba L, Djeghlal ME, Ouallam S, Kahla S. Dissimilar welding of aluminum alloys 2024 T3 and 7075 T6 by TIG process with double tungsten electrodes. Int J Adv Manuf Technol. 2022;118:937-48.
[15] Ouallam S, Masse JE, Peyre P, Djeghlal ML, Guittonneau F, Boutaghou Z, et al. Microstructural and mechanical characterization of the Yb: YAG laser welding of high-pressure die-casting Mg-Al-Mn Magnesium alloy. Int J Eng Res Afr. 2020;51:95-109.
[16] Wang L, Yuan T, Jiang W, Jiang X, Chen S, Liu Y. Microstructure and mechanical properties of dissimilar Mg alloy with Cu interlayer fabricated by pulse current assisted friction stir welding. J Mater Eng Perform. 2023;32(6):2661-75.
[17] Perandini JPB, Bordinassi EC, Batalha MHF, Carunchio AF, Delijaicov S. Superficial residual stress, microstructure, and efficiency in similar joints of AA2024-T3 and AA7475-T761 aluminum alloys formed by friction stir welding. Int J Adv Manuf Technol. 2021;116:117-36.
[18] Patel N, Bhatt KD, Mehta V. Influence of tool pin profile and welding parameter on tensile strength of magnesium alloy AZ91 during FSW. Procedia Technol. 2016;23:558-65.
[19] Kumar KNB, Vanitha C. Microstructural developments and mechanical properties of friction stir welding of AZ91D magnesium alloy plates. Metall Mater Eng. 2017;23(2):119-30.
[20] Çam G. Friction stir welded structural materials: beyond Al-alloys. Int Mater Rev. 2011;56(1):1-48.
[21] Ahmed MM, El-Sayed Seleman MM, Fydrych D, Gürel ÇAM. Review on friction stir welding of dissimilar magnesium and aluminum alloys: Scientometric analysis and strategies for achieving high-quality joints. J Magnes Alloy. 2023;11(11):4082-127.
[22] Mironov S, Onuma T, Sato YS, Kokawa H. Microstructure evolution during friction-stir welding of AZ31 magnesium alloy. Acta Mater. 2015;100:301-12.
[23] Esparza JA, Davis WC, Trillo EA, Murr LE. Friction-stir welding of magnesium alloy AZ31B. J Mater Sci Lett. 2002;21:917-20.

[24] Lee WB, Yeon YM, Jung SB. Joint properties of friction stir welded AZ31B–H24 magnesium alloy. Mater Sci Technol. 2003;19(6):785-90.
[25] Singh K, Singh G, Singh H. Investigation of microstructure and mechanical properties of friction stir welded AZ61 magnesium alloy joint. J Magnes Alloy. 2018;6(3):292-8.
[26] Thimmaiah S, Tener Z, Lamichhane TN, Canfield PC, Miller GJ. Crystal structure, homogeneity range and electronic structure of rhombohedral γ-Mn5Al8. Z Kristallogr-Cryst Mater. 2017;232(7-9):601-10.
[27] Zhang J, Liu H, Chen X, Zou Q, Huang G, Jiang B, et al. Deformation characterization, twinning behavior and mechanical properties of dissimilar friction-stir-welded AM60/AZ31 alloys joint during the three-point bending. Acta Metall Sin (Engl Lett). 2022:35:727-44.
[28] Zhou P, Wang L, Tang H, Cui C, Xu M, Wu D. Microstructure and corrosion resistance of friction stir–welded AZ61A/AZ40M Mg-alloy dissimilar joint. Weld World. 2023;67(1):167-81.
[29] Singh UK, Dubey AK. Welding of dissimilar Mg alloys using indigenously developed friction stir welding set-up. Mater Today Proc. 2021;44:975-8.
[30] Yu Z, Sheng G, Li T. Effect of microstructure and microtexture on mechanical properties and fracture behaviour of friction stir-welded AZ31/AZ61 joint. Mater Res Express. 2018;5(12):125801.
[31] Singh K, Sehgal AK, Singh G, Singh H. Influence of PWHT on FSW joint of AZ61 Mg alloy. Mater Today Proc. 2022;60:2217-21.
[32] Wang Y, Xia M, Fan Z, Zhou X, Thompson GE. The effect of Al8Mn5 intermetallic particles on grain size of as-cast Mg–Al–Zn AZ91D alloy. Intermetallics. 2010;18(8):1683-9.
[33] Cao P, StJohn DH, Qian M. The effect of manganese on the grain size of commercial AZ31 alloy. Mater Sci Forum. 2005; 488-489:139-42.
[34] Huang Y, Wang Y, Meng X, Wan L, Cao J, Zhou L, et al. Dynamic recrystallization and mechanical properties of friction stir processed Mg-Zn-Y-Zr alloys. J Mater Process Technol. 2017;249:331-8.
[35] Wang W, Deng D, Mao Z, Tong Y, Ran Y. Influence of tool rotation rates on temperature profiles and mechanical properties of friction stir welded AZ31 magnesium alloy. Int J Adv Manuf Technol. 2017;88:2191-200.
[36] Unnikrishnan MA, Edwin Raja Dhas J, Anton Savio Lewise K, Varghese JC, Ganesh M. Challenges on friction stir welding of magnesium alloys in automotives. Mater Today Proc. In press 2023.
[37] Heinz B, Skrotzki B. Characterization of a friction-stir-welded aluminum alloy 6013. Metall Mater Trans B. 2002;33(6):489-98.
[38] Commin L. Joining hot-rolled magnesium alloys using friction stir welding and laser beam welding: experimental approach for mechanical properties understanding. Paris: Arts et Métiers; 2008. (In French)
[39] Singh VP, Kuriachen B. Experimental investigations into the mechanical and metallurgical characteristics of friction stir welded AZ31 magnesium alloy. J Mater Eng Perform. 2022;31(12):9812-28.
[40] Kiełbus A, Rzychoń T. Structural stability of Mg–6Al–2Sr magnesium alloy. Solid State Phenomena. 2011;176:75-82.
[41] Liu D, Xin R, Zheng X, Zhou Z, Liu Q. Microstructure and mechanical properties of friction stir welded dissimilar Mg alloys of ZK60–AZ31. Mater Sci Eng A. 2013;561:419-26.
[42] Desai AM, Khatri BC, Patel V, Rana H. Friction stir welding of AZ31 magnesium alloy: a review. Mater Today Proc. 2021;47:6576-84.
[43] Chiuzuli FR, Batistao BF, Bergmann LA, de Alcantara NG, dos Santos JF, Klusemann B, et al. Effect of the gap width in AZ31 magnesium alloy joints obtained by friction stir welding. J Mater Res Technol. 2021;15:5297-306.
[44] Kotari S, Punna E, Gangadhar SM, Cheepu M, Sarkar P, Venukumar S. Dissimilar metals TIG welding-brazing of AZ31 magnesium alloy to 304 stainless steel. Mater Today Proc. 2021;39:1549-52.
[45] Afrin N, Chen DL, Cao X, Jahazi M. Microstructure and tensile properties of friction stir welded AZ31B magnesium alloy. Mater Sci Eng A. 2008;472(1-2),179-86.
[46] Chowdhury SH, Chen DL, Bhole SD, Cao X, Wanjara P. Friction stir welded AZ31 magnesium alloy: microstructure, texture, and tensile properties. Metall Mater Trans A. 2013;44(1):323-36.
[47] Xunhong W, Kuaishe W. Microstructure and properties of friction stir butt-welded AZ31 magnesium alloy. Mater Sci Eng A. 2006;431(1-2):114-7.
[48] Singh K. Effect of post-welding heat treatment on mechanical and microstructural properties of friction stir welded dissimilar magnesium alloys. Mater Today Proc. In press 2023.
[49] Singh VP, Modi A, Kumar A, Kumar D, Mahesh V, Harursampath D, et al. Effect of mix cubic and hexagonal phase on the mechanical and microstructural properties of friction stir welded AZ31 alloy. Mater Lett. 2024;361:136081.
[50] Singh K, Singh G, Singh H. Investigation on the microstructure and mechanical properties of a dissimilar friction stir welded joint of magnesium alloys. Proc Inst Mech Eng Part L: J Mater Des. Appl. 2019;233(12):2444-54.